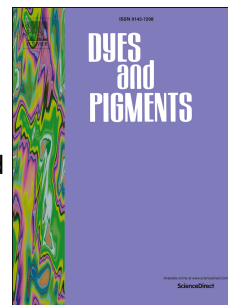


# Accepted Manuscript

Highly efficient and spectrally stable white organic light-emitting diodes using new red heteroleptic Iridium(III) complexes

Hee Un Kim, Jae-Ho Jang, Hea Jung Park, Byung Jun Jung, Wook Song, Jun Yeob Lee, Do-Hoon Hwang



PII: S0143-7208(17)31774-6

DOI: [10.1016/j.dyepig.2017.10.022](https://doi.org/10.1016/j.dyepig.2017.10.022)

Reference: DYPI 6320

To appear in: *Dyes and Pigments*

Received Date: 18 August 2017

Revised Date: 12 October 2017

Accepted Date: 12 October 2017

Please cite this article as: Kim HU, Jang J-H, Park HJ, Jung BJ, Song W, Lee JY, Hwang D-H, Highly efficient and spectrally stable white organic light-emitting diodes using new red heteroleptic Iridium(III) complexes, *Dyes and Pigments* (2017), doi: 10.1016/j.dyepig.2017.10.022.

This is a PDF file of an unedited manuscript that has been accepted for publication. As a service to our customers we are providing this early version of the manuscript. The manuscript will undergo copyediting, typesetting, and review of the resulting proof before it is published in its final form. Please note that during the production process errors may be discovered which could affect the content, and all legal disclaimers that apply to the journal pertain.

# Highly Efficient and Spectrally Stable White Organic Light-Emitting Diodes Using New Red Heteroleptic Iridium(III) Complexes

Hee Un Kim,<sup>a</sup> Jae-Ho Jang,<sup>a</sup> Hea Jung Park,<sup>a</sup> Byung Jun Jung,<sup>b</sup> Wook Song,<sup>c</sup> Jun Yeob Lee,<sup>c</sup>  
and Do-Hoon Hwang<sup>\*,a</sup>

<sup>a</sup> *Department of Chemistry and Chemistry Institute for Functional Materials,*

*Pusan National University, Busan 609-735, Republic of Korea*

<sup>b</sup> *Department of Materials Science and Engineering, The University of Seoul, Seoul 130-743,*

*Republic of Korea*

<sup>c</sup> *School of Chemical Engineering, Sungkyunkwan University, Suwon, Gyeonggi 440-746,*

*Republic of Korea*

\*To whom correspondence should be addressed.

\*E-mail: dohoonhwang@pusan.c.kr

**Abstract**

Highly efficient red phosphorescent iridium(III) complexes,  $(\text{MPQ})_2\text{Ir}(\text{Pppy})$  and  $(\text{MPQ})_2\text{Ir}(\text{TMSppy})$  based on 4-methyl-2-phenylquinoline (MPQ) as a cyclometalated main ligand and 2-[(1,1'-biphenyl)4-yl]pyridine (Pppy) or 2-[4-(trimethylsilyl)phenyl]pyridine (TMSppy) as a second cyclometalated ligand were synthesized for use in organic light-emitting diodes (OLEDs). The iridium(III) complex with MPQ and acetylacetonate (acac) as an ancillary ligand,  $(\text{MPQ})_2\text{Ir}(\text{acac})$ , was also synthesized for comparison. The geometrical configuration of the heteroleptic complex  $(\text{MPQ})_2\text{Ir}(\text{acac})$  is *N,N*-trans, whereas  $(\text{MPQ})_2\text{Ir}(\text{Pppy})$  and  $(\text{MPQ})_2\text{Ir}(\text{TMSppy})$  show all-*facial* geometries. Among the iridium(III) complexes, red OLEDs using the  $(\text{MPQ})_2\text{Ir}(\text{Pppy})$  exhibited significantly more improved luminance and external quantum efficiency with markedly prevented concentration self-quenching at high doping concentration by introduction of Pppy. Moreover, a high maximum external quantum efficiency ( $\text{EQE}_{\text{max}}$ ) of 28.0% with a high color-rendering index (CRI) of 81 was achieved in the white OLEDs (WOLED) fabricated using the bis[2-(4,6-difluorophenyl)pyridinato- $\text{C}^2, \text{N}$ ](picolinato)iridium(III) [FIrpic], tris(2-phenylpyridine)iridium(III) [ $\text{Ir}(\text{ppy})_3$ ], and  $(\text{MPQ})_2\text{Ir}(\text{Pppy})$ , and it is one of the highest values among the reported three primary color component WOLED. Also, the WOLED fabricated using the  $(\text{MPQ})_2\text{Ir}(\text{Pppy})$  showed excellent spectral stability at different voltages.

Keywords: iridium complex; organic light-emitting diodes; phosphorescence

## 1. Introduction

Since the successful commercialization of organic light-emitting diodes (OLEDs) using three primary color emissions in smart phone displays, the market for products such as OLEDs television sets using white OLEDs (WOLED) has expanded [1-5]. Recently, in the fields of WOLED techniques, lighting using WOLED have been attractive due to potentially cheap energy costs and eco-friendly for lighting and various designs as efficient solid-state lighting applications. Also, the use of WOLED techniques in automotive brake light and traffic signal lights is also increasing [6-8].

Generally, WOLED are emitted by combination the two or three (red, green, and blue) primary color components as all-fluorescent, fluorescent-phosphorescent hybrid, and all-phosphorescent methods. Among them, all-phosphorescent three primary color component WOLED give broad white emission and high color-rendering index (CRI) [9-14]. Three primary color component WOLED are desirable in applications such as WOLED televisions because of the high color quality from small light loss after three color filters [15]. The emissive layers in all-phosphorescent WOLED based on three primary color mixing use typical phosphors of blue emitter such as bis[2-(4,6-difluorophenyl)pyridinato- $C^2,N$ ](picolato)iridium(III) [FIrpic], green emitter such as *fac*-tris(2-phenylpyridine)iridium(III) [Ir(ppy)<sub>3</sub>], and red emitter such as bis(2-phenylquinoline)(acetylacetonate)iridium(III) [(pq)<sub>2</sub>Ir(acac)] or bis(1-phenylisoquinoline)(acetylacetonate)iridium(III) [(piq)<sub>2</sub>Ir(acac)] [16-20]. In particular, (pq)<sub>2</sub>Ir(acac) and (piq)<sub>2</sub>Ir(acac) are currently widely used as red emitters in OLEDs because they have suitable red emission regions [21,22]. However, the use of acetylacetonate (acac) as an ancillary ligand in (pq)<sub>2</sub>Ir(acac) or (piq)<sub>2</sub>Ir(acac) causes various problems, such as poor thermal stability, low photoluminescence (PL) quantum efficiency ( $\Phi_{PL}$ ), and concentration

self-quenching at high doping concentrations of organic light-emitting device [23,24]. New red emitter materials with high thermal stabilities, high  $\Phi_{\text{PL}}$  values, and suppressed self-quenching effects are needed to solve these problems for OLEDs applications. Among the previous reports, Lee *et. al.* Reported an iridium(III) complex with a bulky pinene-substituted cyclometalated main ligand to reduce concentration self-quenching at very high dopant concentrations [25].

In this study, we designed new iridium(III) complexes containing a 2-phenylpyridine-based second cyclometalated ligand instead of acac to give high thermal stability and improved quantum efficiency for red and white phosphorescent OLEDs. We identified their geometrical configurations using X-ray crystallography. In general, iridium(III) complexes containing the 2-phenylpyridine ligand have been known to exhibit a broad full width at half maximum (FWHM) and high phosphorescent quantum efficiencies [26]. We synthesized new iridium(III) complexes based on 4-methyl-2-phenylquinoline (MPQ) as the main cyclometalated ligand and 2-[(1,1'-biphenyl)-4-yl]pyridine (Pppy) or 2-[4-(trimethylsilyl)phenyl]pyridine (TMSppy) as the second cyclometalated ligand. Two iridium(III) complexes containing Pppy or TMSppy as the second cyclometalated ligand showed significantly improved thermal stabilities and  $\Phi_{\text{PL}}$  values compared with those of the corresponding iridium(III) complex containing an acac ancillary ligand. We also found that the second cyclometalated ligands are important in preventing self-quenching at high dopant concentrations in red and white phosphorescent OLEDs.

## 2. Experimental Section

### 2.1. Materials

Phenyl boronic acid, 2-chloro-4-methylquinoline, 2-(4-bromophenyl)pyridine, acetylacetone, iridium(III) chloride hydrate, tetrakis(triphenylphosphine)palladium(0), chlorotrimethylsilane, and silver trifluoromethanesulfonate were purchased from Aldrich and Alfa Aesar. All chemicals were used without further purification.

## 2.2. General procedure for iridium(III) complexes

### 2.2.1. Synthesis of 4-methyl-2-phenylquinoline (MPQ)

2-Chloro-4-methylquinoline (5.0 g, 28.1 mmol), phenyl boronic acid (4.12 g, 33.8 mmol), and  $[\text{Pd}(\text{PPh}_3)_4]$  (0.97 g, 0.84 mmol) were dissolved in tetrahydrofuran. A solution of 2M  $\text{K}_2\text{CO}_3$  and Aliquat 336 (1.1 g, 2.72 mmol) was added, and the mixture was refluxed with stirring for 12 h under a nitrogen atmosphere. The reaction mixture was cooled to room temperature, the mixture was extracted with ethyl acetate, and the organic layer was washed with water. The organic layer was dried over  $\text{MgSO}_4$ . The solvent was removed under reduced pressure to give a crude residue. The crude product was purified by column chromatography on silica gel (ethyl acetate/hexane, 1/3, v/v) to obtain MPQ (4.73 g, 76.8%).  $^1\text{H}$  NMR (300 MHz,  $\text{CDCl}_3$ ,  $\delta$ ): 8.18 (m, 3H), 7.97 (d, 1H), 7.78 (t, 1H), 7.70 (s, 1H), 7.53 (m, 4H), 2.75 (s, 3H,  $\text{CH}_3$ );  $^{13}\text{C}$  NMR (75 MHz,  $\text{CDCl}_3$ ,  $\delta$ ): 157.05, 148.14, 144.83, 139.84, 130.29, 129.36, 129.23, 128.82, 127.58, 127.27, 126.05, 123.66, 119.77, 19.02.

### 2.2.2. Synthesis of 2-(4-(phenyl)phenyl)pyridine (Pppy)

Pppy was prepared from 2-(4-bromophenyl)pyridine using the same procedure as was used to synthesize MPQ (2.06 g, 69.6%).  $^1\text{H}$  NMR (300 MHz, acetone- $d_6$ ,  $\delta$ ): 8.70 (d, 1H), 8.25 (d, 2H), 7.98 (d, 1H), 7.90 (t, 1H), 7.78 (m, 4H), 7.49 (t, 2H), 7.41 (d, 1H), 7.33 (m, 1H);  $^{13}\text{C}$

NMR (75 MHz,  $\text{CDCl}_3$ ,  $\delta$ ): 157.01, 149.73, 141.70, 140.56, 138.26, 136.82, 128.87, 127.57, 127.49, 127.34, 127.12, 122.17, 120.49.

### 2.2.3. Synthesis of 2-[4-(trimethylsilyl)phenyl]pyridine (TMSppy)

Under the protection of nitrogen, *n*-BuLi (7.7 mL, 15.4 mmol, 2.0 M solution in hexane) was added dropwise via a syringe to 2-(4-bromophenyl)pyridine (3.0 g, 12.8 mmol) in tetrahydrofuran at  $-78\text{ }^\circ\text{C}$ . The mixture was stirred at  $-78\text{ }^\circ\text{C}$  for 1 h, and chlorotrimethylsilane (2.45 mL, 19.2 mmol) was added in one portion. The reaction mixture was allowed to warm to room temperature overnight. After the reaction mixture was quenched with methanol, the mixture was extracted with ethyl acetate and the organic layer was washed with water. The organic layer was dried over  $\text{MgSO}_4$ . The solvent was removed under reduced pressure to give a crude residue. The crude product was purified by column chromatography on silica gel (ethyl acetate/hexane, 1/3, v/v) to obtain TMSppy (1.86 g, 63.7%).  $^1\text{H}$  NMR (300 MHz,  $\text{CDCl}_3$ ,  $\delta$ ): 7.75 (d, 1H), 7.99 (d, 2H), 7.73 (m, 2H), 7.65 (d, 2H), 7.22 (m, 1H), 0.30 (s, 9H,  $\text{CH}_3$ );  $^{13}\text{C}$  NMR (75 MHz,  $\text{CDCl}_3$ ,  $\delta$ ): 157.45, 149.72, 141.41, 139.70, 136.71, 133.80, 126.13, 122.16, 120.58, 1.08.

### 2.2.4. Synthesis of iridium(III) $\mu$ -chloro bridged dimer $[\text{Ir}(\text{MPQ})_2\text{Cl}]_2$

A mixture of iridium(III) chloride trihydrate (2.0 g, 6.70 mmol) and MPQ (3.23 g, 14.7 mmol) in 2-ethoxyethanol/water (3/1, v/v) was stirred at reflux under a nitrogen atmosphere for 20 h. The mixture was cooled to room temperature and the precipitate was collected and washed with water and petroleum ether several times to afford a dark-red powder. The solid was dried *in vacuo* to give the cyclometalated Iridium(III)  $\mu$ -chloro bridged dimer complex  $[\text{Ir}(\text{MPQ})_2\text{Cl}]_2$ , which was used directly in the next step, without purification.

2.2.5. Synthesis of bis(4-methyl-2-phenylquinoline)iridium(III)(acetylacetonate) ( $(MPQ)_2Ir(acac)$ )

The  $[Ir(MPQ)_2Cl]_2$  dimer complex (0.5g, 0.38 mmol), sodium carbonate (0.39g, 3.76 mmol), and acetylacetonate (0.23 g, 2.26 mmol) were dissolved in 2-ethoxyethanol and refluxed under nitrogen for 12 h. After cooling to room temperature, the crude solution was poured into water, and extracted with dichloromethane/brine. The organic layer was dried over  $MgSO_4$ , and concentrated *in vacuo*. The residue was purified using column chromatography on silica gel with dichloromethane/hexane as the eluent, and then recrystallized in dichloromethane and methanol to afford the product as an orange-red solid (0.17 g, 62.8%).  $^1H$  NMR (300 MHz,  $CDCl_3$ ,  $\delta$ ): 8.52 (d, 2H), 7.97 (d, 2H), 7.86 (s, 2H), 7.78 (d, 2H), 7.47 (m, 4H), 6.85 (t, 2H), 6.58 (t, 2H), 7.54 (d, 2H), 4.62 (s, 1H), 2.92 (s, 6H,  $ArCH_3$ ), 1.54 (s, 3H,  $CH_3$ ), 1.49 (s, 3H,  $CH_3$ );  $^{13}C$  NMR (75 MHz,  $CDCl_3$ ,  $\delta$ ): 185.31, 169.63, 150.88, 147.20, 145.82, 136.04, 129.94, 128.50, 127.21, 127.06, 125.56, 125.53, 123.74, 120.69, 117.40, 99.99, 97.77, 28.32, 19.31; Anal. calcd for  $C_{37}H_{31}IrN_2O_2$ : C; 61.05, H; 4.29, N; 3.85, O; 4.40. Found: C; 61.04, H; 4.29, N; 3.64; MALDI-TOF ( $M^{+1}$ ,  $C_{37}H_{31}IrN_2O_2$ ): calcd for 728.20, found; 728.67; HPLC purity : 99.6%.

2.2.6. Synthesis of bis(4-methyl-2-phenylquinoline)iridium(III)[2-(4-(phenyl)phenyl)pyridine] ( $(MPQ)_2Ir(Pppy)$ )

A solution of silver trifluoromethanesulfonate (0.21 g, 0.83 mmol) in 2-propanol (30 mL) was added to a solution of  $[Ir(MPQ)_2Cl]_2$  dimer complex (0.5 g, 0.38 mmol) in dichloromethane (100 mL). The mixture was stirred at room temperature for overnight. The deep-red solution was filtered with Celite 545 to remove insoluble material and the crude solution was concentrated *in vacuo*. The resulting solid, i.e.,  $[Ir(MPQ)_2(CH_3CN)_2]^+$ triflate] (0.45 g, 0.50mmol) and Pppy (0.17 g, 0.75 mmol) were dissolved in ethanol (200 mL) and

refluxed under nitrogen atmosphere for 16 h. After cooling to room temperature, the crude solution was poured into water, and extracted with dichloromethane/brine; the organic layer was dried over  $\text{MgSO}_4$  and concentrated *in vacuo*. The residue was purified using column chromatography on silica gel with dichloromethane/hexane as the eluent, and then recrystallized in dichloromethane and methanol to afford the product as a red solid (0.29 g, 69.1%).  $^1\text{H}$  NMR (300 MHz,  $\text{CDCl}_3$ ,  $\delta$ ): 8.21 (d, 1H), 8.07 (s, 1H), 8.03 (s, 1H), 7.88 (m, 2H), 7.81 (t, 2H), 7.72 (t, 2H), 7.63 (d, 1H), 7.52 (t, 1H), 7.44 (d, 1H), 7.29 (m, 3H), 6.99 (m, 3H), 6.92 (m, 3H), 6.75 (m, 9H), 2.82 (s, 3H,  $\text{ArCH}_3$ ), 2.76 (s, 3H,  $\text{ArCH}_3$ );  $^{13}\text{C}$  NMR (75 MHz,  $\text{CDCl}_3$ ,  $\delta$ ): 166.9, 166.5, 166.2, 163.8, 160.4, 157.3, 148.6, 148.4, 147.3, 146.9, 145.8, 144.5, 144.3, 144.1, 143.7, 141.8, 141.4, 140.8, 139.6, 138.3, 137.6, 136.8, 130.2, 129.6, 129.5, 129.1, 128.5, 127.9, 127.6, 127.1, 126.2, 125.6, 125.2, 124.8, 124.5, 124.3, 123.6, 122.1, 121.9, 121.1, 119.8, 119.3, 118.9, 118.5, 20.1, 19.8; Anal. Calcd for  $\text{C}_{49}\text{H}_{36}\text{IrN}_3$ : C; 68.51, H; 4.22, N; 4.89. Found: C; 68.56, H; 4.14, N; 4.68; MALDI-TOF ( $\text{M}^+$ ,  $\text{C}_{49}\text{H}_{36}\text{IrN}_3$ ): calcd for 859.25, found; 859.29. HPLC purity : 99.7%.

2.2.7. *Synthesis of bis(4-methyl-2-phenylquinoline)iridium(III)(2-biphenyl-4-yl)[2-(4-trimethylsilyl)phenyl]pyridine] (MPQ)<sub>2</sub>Ir(TMSppy)*

(MPQ)<sub>2</sub>Ir(TMSppy) was prepared from the  $[\text{Ir}(\text{MPQ})_2\text{Cl}]_2$  dimer complex by the same procedure as was used to synthesize (MPQ)<sub>2</sub>Ir(Pppy) (0.28 g, 67.8%).  $^1\text{H}$  NMR (300 MHz,  $\text{CDCl}_3$ ,  $\delta$ ): 8.27 (d, 1H), 8.09 (s, 1H), 7.95 (s, 1H), 7.84 (m, 5H), 7.68 (d, 2H), 7.62 (d, 1H), 7.48 (t, 1H), 7.23 (m, 2H), 6.94 (m, 2H), 6.82 (m, 2H), 6.74 (m, 4H), 6.67 (m, 3H) 2.83 (s, 3H,  $\text{ArCH}_3$ ), 2.74 (s, 3H,  $\text{ArCH}_3$ ), 0.04 (s, 9H,  $\text{CH}_3$ ).  $^{13}\text{C}$  NMR (75 MHz,  $\text{CDCl}_3$ ,  $\delta$ ): 166.5, 166.4, 166.1, 163.5, 160.9, 156.9, 148.7, 148.0, 147.8, 146.6, 145.1, 144.8, 144.3, 144.2, 143.8, 141.2, 141.0, 139.2, 137.0, 136.4, 135.5, 129.8, 129.1, 129.0, 128.2, 127.6, 127.4, 125.8, 125.7, 125.4, 124.6, 124.5, 124.1, 123.6, 121.9, 121.8, 120.0, 119.6, 118.9, 118.7,

118.6, 19.3, 19.1, 1.25. Anal. Calcd for  $C_{46}H_{40}IrN_3Si$ : C; 64.61, H; 4.71, N; 4.91. Found: C; 65.38, H; 4.71, N; 4.82. MALDI-TOF ( $M^{+1}$ ,  $C_{46}H_{40}IrN_3Si$ ): calcd for 855.26, found; 855.73 (HPLC purity : 99.6%.)

### 2.3. Fabrication of red and white OLEDs

#### 2.3.1. Red Phosphorescent OLEDs Fabrication

The device structure of the red OLEDs was ITO (50 nm)/PEDOT:PSS (40 nm)/TAPC (20 nm)/mCP (10 nm)/TCTA:TPBi:red dopant (12.5:12.5:x%)/TSPO1 (35 nm)/LiF (1 nm)/Al (200 nm). In these devices, the red dopants were  $(MPQ)_2Ir(acac)$ ,  $(MPQ)_2Ir(Pppy)$ , and  $(MPQ)_2Ir(TMSppy)$ ; the doping ratio of TCTA to TPBi was 1:1, and the doping concentrations of the red dopants (x%) were 5%, 10%, and 15%. Prior to use, the ITO substrate was cleaned by sonication in distilled water and isopropanol followed by UV/ozone treatment for 10 min. After treatment with oxygen plasma, poly(3,4-ethylenedioxythiophene) doped with poly(styrenesulfonic acid) (PEDOT:PSS, Bayer AG, Germany) was spin-coated onto the cleaned ITO substrates. 1,1-Bis[(di-4-tolylamino)phenyl]cyclohexane (TAPC) and 1,3-bis(N-carbazolyl)benzene (mCP), which serves as the hole-transport layer (HTL), were deposited onto the PEDOT:PSS layer. The red emissive layer was prepared by co-evaporating host TCTA and TPBi with x% red dopant. Next, 4-(triphenylsilyl)phenyldiphenylphosphine oxide (TSPO1), which acts as a high triplet-energy exciton blocking layer (HBL) with electron transport properties, was deposited on the emissive layer. Finally, lithium fluoride (LiF) was deposited as an electron injecting layer (EIL), and aluminum was deposited by vacuum evaporation on top of the film through a mask at less than  $2.0 \times 10^{-6}$  Torr.

#### 2.3.2. White phosphorescent OLEDs Fabrication

The structure of the WOLED was ITO (50 nm)/PEDOT:PSS (40 nm)/TAPC (20 nm)/mCP (10 nm)/mCP:FIrpic (x%):Ir(ppy)<sub>3</sub> (y%)/TCTA:TPBi:red dopant (z%)/TSPO1 (5 nm)/TPBi (30 nm)/LiF (1 nm)/Al (200 nm). The blue, green, and red dopants in W1, W2, and W3 were FIrpic, Ir(ppy)<sub>3</sub>, and red dopant, respectively. The optimal doping concentrations of Ir(ppy)<sub>3</sub> (0.5%) and red dopant (15%) in W1, W2, and W3 were fixed and the doping concentration of FIrpic in each device was controlled from 5% to 15%. The ITO treatment procedure was the same as that for the red phosphorescent OLEDs. PEDOT:PSS was spin-coated onto the cleaned ITO substrates and then TAPC and mCP, which act as a HTL, were deposited onto the PEDOT:PSS layer. A blue and green light emissive layer was prepared by co-evaporating mCP, as the host, and FIrpic and Ir(ppy)<sub>3</sub>, as blue and green dopants, respectively. The red emissive layer was prepared by co-evaporating host TCTA and TPBi, and red dopant. Next, TSPO1 and TPBi, which acts as a high triplet-energy exciton blocking layer with electron transport properties, were deposited on the emissive layer. Finally, LiF was deposited as an EIL, and aluminum was deposited by vacuum evaporation on top of the film through a mask at less than  $2.0 \times 10^{-6}$  Torr.

#### 2.4. Measurements

<sup>1</sup>H and <sup>13</sup>C NMR spectra were recorded in CDCl<sub>3</sub> using a Varian Mercury 300 MHz (75 MHz) spectrometer. MALDI-TOF mass spectra were obtained using a ZMS-DX303 mass spectrometer (JEOL Ltd.). HPLC was performed using a Waters<sup>TM</sup> 600 Controller with a Waters<sup>TM</sup> 486 tunable absorbance detector. TGA was performed using an SDT Q600 V20.9 Build 20 instrument under a nitrogen atmosphere at a heating rate of 10 °C/min. UV-visible absorption spectra were recorded using a Shimadzu UV-3600 spectrophotometer, while PL spectra were recorded on a Shimadzu RF 5301 PC fluorometer. CV was performed using a CH Instruments 600D voltammetric analyzer at a potential scanning rate of 50-100 mV/s at

room temperature in a dichloromethane solution containing 0.1 M tetrabutylammonium perchlorate as the supporting electrolyte. A Ag/AgCl reference electrode, platinum wire counter electrode, and ferrocene/ferrocenium (Fc/Fc<sup>+</sup>) internal standard were used. The J-V-L characteristics and EL spectra of the phosphorescent OLEDs were obtained using a Keithley 2400 source measurement unit and CS 1000 spectrophotometer. All devices were fabricated by vacuum thermal evaporation and were encapsulated with a glass lid and CaO getter before device measurements. A Keithley 2400 source measurement unit and CS 1000 spectroradiometer were used to investigate the device performances. A Lambertian distribution of light emission was assumed in all EQE measurements.

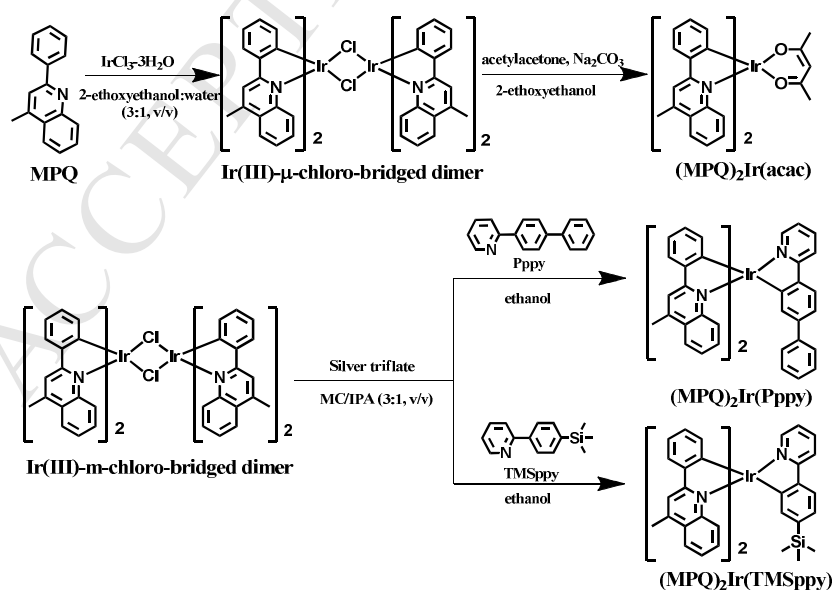
### 3. Results and Discussion

#### 3.1. Synthesis and Thermal Properties

The heteroleptic iridium(III) complexes, (MPQ)<sub>2</sub>Ir(acac), (MPQ)<sub>2</sub>Ir(Pppy), and (MPQ)<sub>2</sub>Ir(TMSppy) were synthesized according to the procedure shown in Scheme 1. The MPQ cyclometalated main ligand was prepared *via* a Suzuki coupling reaction between 2-chloro-4-methylquinoline and phenylboronic acid. The second cyclometalated ligands, i.e., Pppy and TMSppy, were prepared from 2-(4-bromophenyl)pyridine and phenylboronic acid or chlorotrimethylsilane, respectively, *via* a Suzuki coupling or silylation reaction. (MPQ)<sub>2</sub>Ir(acac) was synthesized using the conventional two-step reaction reported by Thompson's group [22]. The Ir(III)- $\mu$ -chloro-bridged dimer was formed by reaction of the cyclometalated main ligand MPQ with IrCl<sub>3</sub>·H<sub>2</sub>O in a mixture of 2-ethoxyethanol and water (3:1, v/v). The Ir(III)- $\mu$ -chloro-bridged dimer was then reacted with acac in 2-ethoxyethanol to afford (MPQ)<sub>2</sub>Ir(acac) in 63%. In the syntheses of (MPQ)<sub>2</sub>Ir(Pppy) and (MPQ)<sub>2</sub>Ir(TMSppy), a solution of silver trifluoromethanesulfonate in 2-propanol was added to a solution of the Ir(III)- $\mu$ -chloro-bridged dimer in dichloromethane and the mixture was

stirred at room temperature for 12 h. It was then reacted at 80 °C for 12 h with 2.2 equiv. of Pppy or TMSppy in ethanol to give  $(\text{MPQ})_2\text{Ir}(\text{Pppy})$  and  $(\text{MPQ})_2\text{Ir}(\text{TMSppy})$  in yields of 69% and 68%, respectively. The synthesized iridium(III) complexes were fully characterized using  $^1\text{H}$  and  $^{13}\text{C}$  NMR spectroscopies, elementary analysis, and matrix-assisted laser desorption/ionization time-of-flight (MALDI-TOF) mass spectrometry (see Figure S1 in the Supporting Information). They were purified by the vacuum sublimation using a train sublimator before device fabrication. High-performance liquid chromatography (HPLC) analysis showed that their purities were greater than 99.6% (Figure S2).

The thermal stabilities of  $(\text{MPQ})_2\text{Ir}(\text{acac})$ ,  $(\text{MPQ})_2\text{Ir}(\text{Pppy})$ , and  $(\text{MPQ})_2\text{Ir}(\text{TMSppy})$  were investigated using thermogravimetric analysis (TGA). The 5% weight-loss temperatures ( $T_d$ ) of  $(\text{MPQ})_2\text{Ir}(\text{acac})$ ,  $(\text{MPQ})_2\text{Ir}(\text{Pppy})$ , and  $(\text{MPQ})_2\text{Ir}(\text{TMSppy})$  were 367, 415, and 406 °C, respectively (Figure S3). The  $T_d$  values show that the iridium(III) complexes with Pppy or TMSppy as the second cyclometalated ligand are thermally more stable than the corresponding iridium(III) complex containing acac as the ancillary ligand.



**Scheme 1.** Synthesis and chemical structures of  $(\text{MPQ})_2\text{Ir}(\text{acac})$ ,  $(\text{MPQ})_2\text{Ir}(\text{Pppy})$ , and  $(\text{MPQ})_2\text{Ir}(\text{TMSppy})$ .

### 3.2. X-ray Crystallography

The structures of (MPQ)<sub>2</sub>Ir(acac), (MPQ)<sub>2</sub>Ir(Pppy), and (MPQ)<sub>2</sub>Ir(TMSppy) were investigated using single-crystal X-ray crystallography. Figure 1 and Table 1 shows the single crystal and crystal packing structure of (MPQ)<sub>2</sub>Ir(acac), (MPQ)<sub>2</sub>Ir(Pppy), and (MPQ)<sub>2</sub>Ir(TMSppy) as well as the selected bond lengths. The crystal structures of the iridium(III) complexes with acac or 2-phenylpyridine-based second cyclometalated ligands show different configurations with distorted octahedral geometries around the iridium(III) atom. The geometrical configuration of the heteroleptic complex (MPQ)<sub>2</sub>Ir(acac) is *N,N*-trans, whereas (MPQ)<sub>2</sub>Ir(Pppy) and (MPQ)<sub>2</sub>Ir(TMSppy) have *facial* geometries. All the  $\sigma$ -donor carbon atoms in (MPQ)<sub>2</sub>Ir(Pppy) (C11, C33, and C49) and (MPQ)<sub>2</sub>Ir(TMSppy) (C16, C32, and C40) are located trans to nitrogen atoms (N1, N2, and N3) in both the cyclometalated main ligand and second cyclometalated ligands. The lengths of Ir-C bonds between the iridium atom and two cyclometalated main ligands in (MPQ)<sub>2</sub>Ir(Pppy) [Ir(1)-C(33); 1.985(8) Å, Ir(1)-C(49); 2.000(8) Å] and (MPQ)<sub>2</sub>Ir(TMSppy) [Ir(1)-C(16); 2.012(4) Å, Ir(1)-C(32); 2.007(4) Å] are slightly longer than those in (MPQ)<sub>2</sub>Ir(acac) [Ir(1)-C(16); 1.978(5) Å, Ir(1)-C(27); 1.973(5) Å]. Also, the lengths of the Ir-N bonds in (MPQ)<sub>2</sub>Ir(Pppy) [Ir(1)-N(2); 2.181(6) Å, Ir(1)-N(3); 2.224(7) Å] and (MPQ)<sub>2</sub>Ir(TMSppy) [Ir(1)-N(1); 2.236(3) Å, Ir(1)-N(2); 2.198(3) Å] are also relatively longer than that in (MPQ)<sub>2</sub>Ir(acac) [Ir(1)-N(1); 2.063(4) Å, Ir(1)-N(2); 2.069(4) Å]; this could be because the steric hindrance effects of the second cyclometalated ligand spacers with relatively bulky Pppy or TMSppy groups are greater than that of the acac ancillary ligand. The Ir-C and Ir-N bonds between the iridium atom and second cyclometalated ligands in (MPQ)<sub>2</sub>Ir(Pppy) [Ir(1)-C(11); 2.015(8) Å, Ir(1)-N(1);

2.142(6) Å] and (MPQ)<sub>2</sub>Ir(TMSppy) [Ir(1)-C(40); 2.009(4) Å, Ir(1)-N(3); 2.145(3) Å] were similar.

The distances between the two nearest iridium atoms in the crystal-packing structures of (MPQ)<sub>2</sub>Ir(acac), (MPQ)<sub>2</sub>Ir(Pppy), and (MPQ)<sub>2</sub>Ir(TMSppy) are 10.80, 15.32, and 10.94 Å, respectively. The distances between the two nearest parallel MPQ planes in (MPQ)<sub>2</sub>Ir(acac), (MPQ)<sub>2</sub>Ir(Pppy), and (MPQ)<sub>2</sub>Ir(TMSppy) are 3.43, 9.74, and 3.49 Å, respectively. In particular, the distance between the two nearest iridium atoms and two nearest parallel MPQ planes in (MPQ)<sub>2</sub>Ir(Pppy) are relatively longer than those in (MPQ)<sub>2</sub>Ir(acac) and (MPQ)<sub>2</sub>Ir(TMSppy). These results indicate that (MPQ)<sub>2</sub>Ir(Pppy) has weak intermolecular  $\pi$ - $\pi$  interactions between the two nearest iridium atoms and two nearest MPQ ligands, which could minimize bimolecular interactions by sterically hindered Pppy spacers. Minimum bimolecular interactions between iridium(III) complexes can generally prevent self-quenching in phosphorescence [25]. Complete crystal data (cif) for (MPQ)<sub>2</sub>Ir(acac), (MPQ)<sub>2</sub>Ir(Pppy), and (MPQ)<sub>2</sub>Ir(TMSppy) can be found in Supporting Information.

### 3.3. Photophysical Properties

The photophysical properties of the iridium(III) complexes with second cyclometalated ligands were investigated using UV-visible absorption and PL spectroscopy in dilute toluene solution at 298 K. The UV-visible absorption and PL spectra are shown in Figure 2, and the results are summarized in Table 2. The intense absorption peaks in the short wavelength region below 340 nm in the spectra of all the synthesized iridium(III) complexes are attributed to spin allowed  $\pi$ - $\pi^*$  transitions, which closely resembles the corresponding transition in the MPQ cyclometalated main ligand. (MPQ)<sub>2</sub>Ir(acac) has absorption bands with low extinction coefficients in the range 350-600 nm; these are assigned to singlet and triplet

metal-to-ligand charge transfer ( $^1\text{MLCT}$  and  $^3\text{MLCT}$ ) states. The  $^1\text{MLCT}/^3\text{MLCT}$  bands of the iridium(III) complexes with second cyclometalated ligands are highly and clearly separated, at 398/446 nm for  $(\text{MPQ})_2\text{Ir}(\text{Pppy})$  and 402/450 nm for  $(\text{MPQ})_2\text{Ir}(\text{TMSppy})$ .  $(\text{MPQ})_2\text{Ir}(\text{Pppy})$  and  $(\text{MPQ})_2\text{Ir}(\text{TMSppy})$  show a high and prominent absorption band above 350 nm, from efficient MLCT. The energy band gaps ( $E_g$ ) of  $(\text{MPQ})_2\text{Ir}(\text{acac})$ ,  $(\text{MPQ})_2\text{Ir}(\text{Pppy})$ , and  $(\text{MPQ})_2\text{Ir}(\text{TMSppy})$  were calculated to be 2.09, 2.14, and 2.12 eV, respectively, from the UV-visible absorption edge.

The maximum PL emission peaks of  $(\text{MPQ})_2\text{Ir}(\text{acac})$ ,  $(\text{MPQ})_2\text{Ir}(\text{Pppy})$ , and  $(\text{MPQ})_2\text{Ir}(\text{TMSppy})$  occur at 589, 597, and 597 nm, respectively, in dilute toluene solution at 298 K. The maximum PL emission peaks from  $(\text{MPQ})_2\text{Ir}(\text{Pppy})$  and  $(\text{MPQ})_2\text{Ir}(\text{TMSppy})$  are red-shifted compared with that of  $(\text{MPQ})_2\text{Ir}(\text{acac})$ . Also, red-shifts of the maximum PL emission peaks from solution to the neat film state were observed for  $(\text{MPQ})_2\text{Ir}(\text{acac})$  (595 nm),  $(\text{MPQ})_2\text{Ir}(\text{Pppy})$  (601 nm), and  $(\text{MPQ})_2\text{Ir}(\text{TMSppy})$  (602 nm); this could be caused by aggregation effects of the iridium(III) complexes.

The maximum low-temperature PL emission peaks of  $(\text{MPQ})_2\text{Ir}(\text{acac})$ ,  $(\text{MPQ})_2\text{Ir}(\text{Pppy})$ , and  $(\text{MPQ})_2\text{Ir}(\text{TMSppy})$  in dilute toluene solution at 77 K are at 580, 576, and 578 nm, respectively (Figure S4). The maximum emissions of  $(\text{MPQ})_2\text{Ir}(\text{acac})$ ,  $(\text{MPQ})_2\text{Ir}(\text{Pppy})$ , and  $(\text{MPQ})_2\text{Ir}(\text{TMSppy})$  at 77 K are hypsochromically shifted by 9, 19, and 18 nm compared to those of a solution at 298 K, because of the rigidochromic effect [27-29]. Also, the maximum emission wavelength at 77 K for  $(\text{MPQ})_2\text{Ir}(\text{Pppy})$  and  $(\text{MPQ})_2\text{Ir}(\text{TMSppy})$  are relatively more hypsochromically shifted than that of  $(\text{MPQ})_2\text{Ir}(\text{acac})$ , because of the steric effects of the relatively bulky Pppy and TMSppy groups. The triplet energies ( $T_1$ ) of  $(\text{MPQ})_2\text{Ir}(\text{acac})$ ,  $(\text{MPQ})_2\text{Ir}(\text{Pppy})$ , and  $(\text{MPQ})_2\text{Ir}(\text{TMSppy})$  are 2.14, 2.13, and 2.13 eV, respectively, determined from their emission spectra at 77 K, suggesting that the  $T_1$  energies of the synthesized iridium(III) complexes mainly depend on the cyclometalated MPQ ligand.

The PL quantum yields of the synthesized iridium(III) complexes in dilute degassed 2-methyltetrahydrofuran solution were compared with that of (pq)<sub>2</sub>Ir(acac) as a standard ( $\Phi_{\text{PL}} = 0.10$ ) [30]. The measured  $\Phi_{\text{PL}}$  values of (MPQ)<sub>2</sub>Ir(acac), (MPQ)<sub>2</sub>Ir(Pppy), and (MPQ)<sub>2</sub>Ir(TMSppy) were 0.11, 0.16, and 0.13, respectively. The higher  $\Phi_{\text{PL}}$  values of (MPQ)<sub>2</sub>Ir(Pppy) and (MPQ)<sub>2</sub>Ir(TMSppy) compared with those of (MPQ)<sub>2</sub>Ir(acac) and (PQ)<sub>2</sub>Ir(acac) suggest that the second cyclometalated ligands are better than the acac ancillary ligand at enhancing the PL quantum efficiencies of the red emitters. In particular, Pppy is an excellent candidate as the second cyclometalated ligand for highly luminescent iridium(III) complexes.

### 3.4. Theoretical Calculations

We performed theoretical calculations based on density functional theory (DFT), using the B3LYP hybrid exchange-correlation functional and 6-31G(d) basis sets, to improve our understanding of the effects of Pppy and TMSppy second cyclometalated ligands in iridium(III) complexes. The calculations were conducted using the Gaussian 09 package [31]. Figure 3 shows the electron distributions and calculated energy levels of the highest occupied molecular orbital (HOMO) and lowest unoccupied molecular orbital (LUMO) for (MPQ)<sub>2</sub>Ir(acac), (MPQ)<sub>2</sub>Ir(Pppy), and (MPQ)<sub>2</sub>Ir(TMSppy). The electron densities in the HOMO of (MPQ)<sub>2</sub>Ir(acac) are mainly distributed over the phenyl ring in MPQ and the iridium atom, and the LUMO is mostly distributed over the quinoline moiety. In most cases, the acac ancillary ligand in the iridium(III) complex does not affect the HOMO and LUMO distributions. However, in the case of (MPQ)<sub>2</sub>Ir(Pppy) and (MPQ)<sub>2</sub>Ir(TMSppy), the electron densities in the HOMOs are mainly localized on the phenyl rings of the MPQ moieties, iridium atoms, and phenyl units in the second cyclometalated ligands (Pppy and TMSppy). In contrast, the electron densities in the LUMOs are mainly distributed over the quinoline

moiety, as in  $(\text{MPQ})_2\text{Ir}(\text{acac})$ . The theoretical calculations show that the Pppy and TMSppy second cyclometalated ligands do not contribute to the LUMOs, but selectively contribute to the HOMOs of the iridium(III) complexes.

The calculated HOMO/LUMO energy levels of  $(\text{MPQ})_2\text{Ir}(\text{acac})$ ,  $(\text{MPQ})_2\text{Ir}(\text{Pppy})$ , and  $(\text{MPQ})_2\text{Ir}(\text{TMSppy})$  were -4.84/-1.65, -4.80/-1.59, and -4.79/-1.58 eV, respectively. The HOMO and LUMO energy levels of the iridium(III) complexes containing second cyclometalated ligands were slightly higher than those of the iridium(III) complex containing the acac ancillary ligand.

### 3.5. Electrochemical Properties

The electrochemical behaviors in dichloromethane of the synthesized iridium(III) complexes were investigated using cyclic voltammetry; the results are shown in Figure S5.  $(\text{MPQ})_2\text{Ir}(\text{acac})$ ,  $(\text{MPQ})_2\text{Ir}(\text{Pppy})$ , and  $(\text{MPQ})_2\text{Ir}(\text{TMSppy})$  show reversible electron oxidations at positive potentials in the region 0.40-0.60 V. The onset potentials of the first oxidations ( $E_{\text{onset}}^{\text{oxi}}$ ) of  $(\text{MPQ})_2\text{Ir}(\text{acac})$ ,  $(\text{MPQ})_2\text{Ir}(\text{Pppy})$ , and  $(\text{MPQ})_2\text{Ir}(\text{TMSppy})$  are at 0.49, 0.44, and 0.41 V (vs  $\text{Ag}/\text{Ag}^+$ ), respectively. The  $E_{\text{onset}}^{\text{oxi}}$  values of  $(\text{MPQ})_2\text{Ir}(\text{Pppy})$  and  $(\text{MPQ})_2\text{Ir}(\text{TMSppy})$  are clearly lower than that of the parent complex  $(\text{MPQ})_2\text{Ir}(\text{acac})$ . The HOMO energy levels of  $(\text{MPQ})_2\text{Ir}(\text{acac})$ ,  $(\text{MPQ})_2\text{Ir}(\text{Pppy})$ , and  $(\text{MPQ})_2\text{Ir}(\text{TMSppy})$  are -5.21, -5.16, and -5.13 eV, respectively. The HOMO energy levels of the iridium(III) complexes containing second cyclometalated ligands are slightly higher than those of  $(\text{MPQ})_2\text{Ir}(\text{acac})$ . The LUMO energy levels of  $(\text{MPQ})_2\text{Ir}(\text{acac})$ ,  $(\text{MPQ})_2\text{Ir}(\text{Pppy})$ , and  $(\text{MPQ})_2\text{Ir}(\text{TMSppy})$  are -3.12, -3.02, and -3.01 eV, respectively, based on a combination of the HOMO energy levels and optical band gaps. These HOMO and LUMO energy levels for the iridium(III) complexes are consistent with the theoretically calculated results.

These HOMO and LUMO energy levels are well matched with those of tris(4-carbazoyl-9-ylphenyl)amine (TCTA; HOMO: -6.0 eV, LUMO: -2.70 eV) and 1,3,5-tris(1-phenyl-1*H*-benzimidazol-2-yl)benzene (TPBi; HOMO: -6.70 eV, LUMO: -2.70 eV) as host materials. The HOMO and LUMO energy levels of the iridium(III) complexes are summarized in Table 2.

### 3.6. Electrophosphorescent OLEDs

The performances of the synthesized iridium(III) complexes in red phosphorescent OLEDs were evaluated by fabricating multi-layered devices with the structure ITO (50 nm)/PEDOT:PSS (40 nm)/TAPC (20 nm)/mCP (10 nm)/TCTA:TPBi:red dopant (12.5:12.5:x%)/TSPO1 (35 nm)/LiF (1 nm)/Al (200 nm). We fabricated devices using TCTA and TPBi as the mixed-hosts in the emissive layer for efficient carrier injection and charge balance [32]. Doping concentrations of 5% for (MPQ)<sub>2</sub>Ir(acac), 15% for (MPQ)<sub>2</sub>Ir(Pppy), and 15% for (MPQ)<sub>2</sub>Ir(TMSppy) gave the optimal performances. The doping concentration of iridium(III) complexes with Pppy or TMSppy second cyclometalated ligands were higher than that of the iridium(III) complex containing an acac ancillary ligand. It has been known that the thermally evaporated iridium complex host would exist as an aggregated form rather than a discrete molecule in the host-guest thin film even at low doping concentration [33]. So the above results suggest that the introduction of relatively bulky Pppy or TMSppy groups into the iridium(III) complex effectively suppresses concentration self-quenching especially at high doping concentrations. The various doping concentrations and detailed device characteristics of (MPQ)<sub>2</sub>Ir(acac), (MPQ)<sub>2</sub>Ir(Pppy), and (MPQ)<sub>2</sub>Ir(TMSppy) are summarized in Table 3.

Figure 4a shows that the optimized red phosphorescent OLEDs fabricated using  $(\text{MPQ})_2\text{Ir}(\text{acac})$ ,  $(\text{MPQ})_2\text{Ir}(\text{Pppy})$ , and  $(\text{MPQ})_2\text{Ir}(\text{TMSppy})$  have electroluminescent (EL) maximum emission peaks at 592, 600, and 600 nm, respectively. The maximum emission peaks of the  $(\text{MPQ})_2\text{Ir}(\text{acac})$ ,  $(\text{MPQ})_2\text{Ir}(\text{Pppy})$ , and  $(\text{MPQ})_2\text{Ir}(\text{TMSppy})$  devices red-shift slightly as the doping concentration increases from 5% to 15%; this may be the result of increased dopants aggregation and strong intermolecular interactions at high doping concentration (Figure S6). The red-shifts of the maximum emission peaks at high doping concentrations of all the synthesized iridium(III) complexes are consistent with the aggregation effect observed for neat films, described in photophysical properties. The Commission Internationale de L'Eclairage (CIE) coordinates of the  $(\text{MPQ})_2\text{Ir}(\text{acac})$ ,  $(\text{MPQ})_2\text{Ir}(\text{Pppy})$ , and  $(\text{MPQ})_2\text{Ir}(\text{TMSppy})$  devices at the optimal doping concentration are observed to be (0.59,0.41), (0.60,0.40), and (0.58,0.41), respectively, at 1,000  $\text{cd/m}^2$ .

Figure 4b shows the current density-voltage-luminance (J-V-L) curves of the red phosphorescent OLEDs. The current density of the OLEDs increased with increases doping concentration of  $(\text{MPQ})_2\text{Ir}(\text{Pppy})$  and  $(\text{MPQ})_2\text{Ir}(\text{TMSppy})$ , due to improved charge hopping at high doping concentrations [34]. The turn-on voltage ( $V_{\text{turn-on}}$ ; defined as the bias at a luminance of 1  $\text{cd/m}^2$ ) and maximum luminance ( $L_{\text{max}}$ ) of the  $(\text{MPQ})_2\text{Ir}(\text{acac})$  device are 4.5 V and 5,235  $\text{cd/m}^2$ , respectively. On the other hand,  $(\text{MPQ})_2\text{Ir}(\text{Pppy})$  and  $(\text{MPQ})_2\text{Ir}(\text{TMSppy})$  dramatically change the device performances of red phosphorescent OLEDs. The  $V_{\text{turn-on}}$  and  $L_{\text{max}}$  values of the iridium(III) complexes with second cyclometalated ligands are 4.0 V and 14,690  $\text{cd/m}^2$ , respectively, for the  $(\text{MPQ})_2\text{Ir}(\text{Pppy})$  device, and 3.5 V and 12,220  $\text{cd/m}^2$  for the  $(\text{MPQ})_2\text{Ir}(\text{TMSppy})$  device.

Figure 4c shows the external quantum efficiency-L-current efficiency (EQE-L-CE) curves of red phosphorescent OLEDs. The maximum external quantum efficiency ( $\text{EQE}_{\text{max}}$ )/maximum current efficiency ( $\text{CE}_{\text{max}}$ ) of the  $(\text{MPQ})_2\text{Ir}(\text{acac})$  device is 11.1%/20.4  $\text{cd/A}$ , and those of the

(MPQ)<sub>2</sub>Ir(Pppy) and (MPQ)<sub>2</sub>Ir(TMSppy) devices are 21.4%/35.5 cd/A and 18.4%/31.8 cd/A, respectively. In particular, the EQE<sub>max</sub> and CE<sub>max</sub> values of the (MPQ)<sub>2</sub>Ir(Pppy) device are higher than those of (MPQ)<sub>2</sub>Ir(acac) and (MPQ)<sub>2</sub>Ir(TMSppy). These results show that the iridium(III) complex with a Pppy second cyclometalated ligand significantly improves the EQE and CE compared with the corresponding acac ancillary ligand and TMSppy second cyclometalated ligand. These results can be explained by significant weak intermolecular  $\pi$ - $\pi$  interactions for (MPQ)<sub>2</sub>Ir(Pppy), as described in the X-ray crystallography measurement. The weak intermolecular  $\pi$ - $\pi$  interactions of (MPQ)<sub>2</sub>Ir(Pppy) can effectively prevent concentration self-quenching at high doping concentration and suppress triplet-triplet annihilation in the device [25]. Relatively high  $\Phi_{\text{PL}}$  of the (MPQ)<sub>2</sub>Ir(Pppy) emitter compared with those of the other emitters is another factor for the high EQE of the (MPQ)<sub>2</sub>Ir(Pppy) device. The device characteristics at other doping concentrations of (MPQ)<sub>2</sub>Ir(acac), (MPQ)<sub>2</sub>Ir(Pppy), and (MPQ)<sub>2</sub>Ir(TMSppy) are shown in Figure S7 and S8.

The (MPQ)<sub>2</sub>Ir(Pppy) emitter, which displayed broad FWHM and high EQE values in red phosphorescent OLEDs, is an appropriate red emitter for the fabrication of all-phosphorescent three primary color component WOLED with high EQE and high CRI. We developed WOLED that incorporated FIrpic, Ir(ppy)<sub>3</sub>, and (MPQ)<sub>2</sub>Ir(Pppy) as emissive dopants at different doping concentrations. The three device structures, i.e., W1, W2, and W3, were ITO (50 nm)/PEDOT:PSS (40 nm)/TAPC (20 nm)/mCP (10 nm)/mCP:FIrpic (12.5 nm, x = 5% for W1, 10% for W2, 15% for W3):Ir(ppy)<sub>3</sub> (0.5%)/TCTA:TPBi:(MPQ)<sub>2</sub>Ir(Pppy) (7.25 nm, 15%)/TSPO1 (5 nm)/TPBi (30 nm)/LiF (1 nm)/Al (200 nm). The doping concentrations of Ir(ppy)<sub>3</sub> (0.5%) and (MPQ)<sub>2</sub>Ir(Pppy) (15%) in all white devices were fixed, and the doping concentration of FIrpic in each device was controlled at 5%, 10% and 15% for W1, W2 and W3, respectively. Figure 5a shows the EL spectra of the WOLED fabricated with (MPQ)<sub>2</sub>Ir(Pppy). The white EL spectra show blue, green, and red emission peaks at 473,

505, and 600 nm, respectively. These three emission peaks well match the peak wavelengths of FIrpic, Ir(ppy)<sub>3</sub>, and (MPQ)<sub>2</sub>Ir(Pppy), respectively. The CIE coordinates of W1, W2, and W3 are (0.47,0.42), (0.46,0.43), and (0.44,0.44), respectively, at 1,000 cd/m<sup>2</sup>, and are close to the CIE coordinates of standard warm white light (0.44,0.40). The correlated color temperature (CCT) values of W1, W2, and W3 are 2605, 2932, and 3283 K, respectively, at 1,000 cd/m<sup>2</sup>. Devices W1, W2, and W3 showed intense and broad white emissions with CRI of 78, 81, and 81, respectively. The CRI values of the WOLED device with (MPQ)<sub>2</sub>Ir(Pppy) are therefore greater than the required CRI value of at least 75 for a WOLED to be used in general solid-state lighting application [35]. The J-V-L and EQE-L-power efficiency (EQE-L-PE) characteristics of the WOLED are shown in Figure 5b and 5c, and details of the performances of the EL devices are summarized in Table 4. The V<sub>turn-on</sub> values of the W1, W2, and W3 devices are 6.0, 5.5, and 5.5 V, and the L<sub>max</sub> values are 28,040, 34,500, and 38,320 cd/m<sup>2</sup>, respectively. The EQE and PE values are the most important requirements of WOLED for lighting applications. The EQE<sub>max</sub> and maximum power efficiency (PE<sub>max</sub>) values of W1, W2, and W3 are 22.6%/19.5 lm/W, 26.1%/23.2 lm/W, and 28.0%/26.0 lm/W, respectively. An EQE<sub>max</sub> value of 28.0% was obtained for the W3 device. Table 5 shows the EQE<sub>max</sub> and CIE coordinates of this work as well as those of other WOLEDs reported in the literature [17, 36-43]. The EQE<sub>max</sub> of the W3 device is the highest value among the reported WOLEDs fabricated using three primary color components.

The WOLED color stability is also important in real applications. We investigated the color stability, by observing the EL spectra and CIE coordinates of W1-W3 at various driving voltages from 8 to 12 V. As can be seen from Figure S10, the white EL spectra of the WOLED were not significantly different at different driving voltages. Changes in the CIE coordinates of W1-W3 at various driving voltages were also investigated, as shown in Figure 6. The CIE-X and CIE-Y values of W1-W3 with increasing driving voltage from 8 to 12 V

were similar. Especially, the CIE coordinates of W3 (0.44, 0.44) were unchanged at different driving voltages.

#### 4. Conclusions

In conclusion, red phosphorescent iridium(III) complexes,  $(\text{MPQ})_2\text{Ir}(\text{Pppy})$  and  $(\text{MPQ})_2\text{Ir}(\text{TMSppy})$ , were designed and successfully synthesized to investigate the effect of second cyclometalated Pppy and TMSppy ligands on their use in phosphorescent OLEDs. The devices fabricated using  $(\text{MPQ})_2\text{Ir}(\text{Pppy})$  and  $(\text{MPQ})_2\text{Ir}(\text{TMSppy})$  exhibited EQE of 21.4% and 18.4%, respectively, at 15% doping concentration. Especially, the second cyclometalated Pppy ligand prevented concentration self-quenching and suppressed triplet-triplet annihilation at high doping concentration. The WOLED fabricated using  $(\text{MPQ})_2\text{Ir}(\text{Pppy})$  exhibited the highest EQE of 28.0%. Especially, CIE-X and CIE-Y values at different driving voltages of the WOLED fabricated with  $(\text{MPQ})_2\text{Ir}(\text{Pppy})$  showed excellent spectral stability.

#### Acknowledgements

This work was supported by the Ministry of Trade, Industry and Energy (MOTIE, Korea) under Industrial Technology Innovation Program (No. 10067715), and National Research Foundation (NRF) grants, funded by the Korean government (NRF-2014R1A2A2A01007318 and No. 2011-0030013 through GCRC SOP).

#### References

- [1] Forrest SR. The path to ubiquitous and low-cost organic electronic appliances on plastic. Nature 2004;428:911-8.

- [2] Baldo MA, O'Brien DF, You Y, Shoustikov A, Sibley S, Thompson ME, Forrest SR. Highly efficient phosphorescent emission from organic electroluminescent devices. *Nature* 1988;395:151-4.
- [3] Ouyang X, Li XL, Ai L, Mi D, Ge Z, Su SJ. Novel "hot exciton" blue fluorophores for high performance fluorescent/phosphorescent hybrid white organic light-emitting diodes with superhigh phosphorescent dopant concentration and improved efficiency roll-off. *ACS Appl Mater Interfaces* 2015;7:7869-77.
- [4] Li XL, Ouyang X, Liu M, Ge Z, Peng J, Cao Y, Su SJ. Highly efficient single- and multi-emission-layer fluorescent/phosphorescent hybrid white organic light-emitting diodes with ~20% external quantum efficiency. *J Mater Chem C* 2015;3:9233-9.
- [5] Xu H, Chen R, Sun Q, Lai W, Su Q, Huang W, Liu X. Recent progress in metal-organic complexes for optoelectronic applications. *Chem Soc Rev* 2014;43:3259-302.
- [6] Farinola GM, Ragni R. Electroluminescent materials for white organic light emitting diodes. *Chem Soc Rev* 2011;40:3467-82.
- [7] Sasabe H, Kido J. Development of high performance OLEDs for general lighting. *J Mater Chem C* 2013;1:1699-707.
- [8] D'Andrade BW, Forrest SR. White organic light-emitting devices for solid-state lighting. *Adv Mater* 2004;16:1585-95.
- [9] Wang Q, Ding J, Ma D, Cheng Y, Wang L, Jing X, Wang F. Harvesting excitons via two parallel channels for efficient white organic LEDs with nearly 100% internal quantum efficiency: fabrication and emission-mechanism analysis. *Adv Funct Mater* 2009;19: 84-95.
- [10] Wu H, Ying L, Yang W, Cao Y. Progress and perspective of polymer white light-emitting devices and materials. *Chem Soc Rev* 2009;38:3391-400.

- [11] Zou J, Wu H, Lam CS, Wang C, Zhu J, Zhong C, Hu S, Ho CL, Zhou GJ, Wu H, Choy WCH, Peng J, Cao Y, Wong WY. Simultaneous optimization of charge-carrier balance and luminous efficacy in highly efficient white polymer light-emitting devices. *Adv Mater* 2011;23:2976-80.
- [12] Sun Y, Forrest SR. High-efficiency white organic light emitting devices with three separate phosphorescent emission layers. *Appl Phys Lett* 2007;91:263503/1-3.
- [13] Han C, Zhu L, Li J, Zhao F, Zhang Z, Xu H, Deng Z, Ma D, Yan P. Highly efficient multifuorenyl host materials with unsymmetrical molecular configurations and localized triplet states for green and red phosphorescent devices. *Adv Mater* 2014;26:7070-7.
- [14] Han F, Zhang X, Zhang J, Wei Y, Zhang X, Huang W, Xu H. 3D-Encapsulated iridium-complexed nanophosphors for highly efficient host-free organic light-emitting diodes. *Chem Commun* 2016;52:5183-6.
- [15] Chang CH, Cheng HC, Lu YJ, Tien KC, Lin HW, Lin CL, Yang CJ, Wu CC. Enhancing color gamut of white OLED displays by using microcavity green pixels. *Org Electron* 2010;11:247-54.
- [16] Chang YL, Song Y, Wang Z, Helander MG, Qiu J, Chai L, Liu Z, Scholes GD, Lu Z. Highly efficient warm white organic light-emitting diodes by triplet exciton conversion. *Adv Funct Mater* 2013;23:705-12.
- [17] Zhao Y, Chen J, Ma D. Ultrathin nondoped emissive layers for efficient and simple monochrome and white organic light-emitting diodes. *ACS Appl Mater Interfaces* 2013;5:965-71.
- [18] Kim YH, Cheah KW, Kim YY. High efficient white organic light-emitting diodes with single emissive layer using phosphorescent red, green, and blue dopants. *Appl Phys Lett* 2013;103:053307/1-4.

- [19] Wang Q, Ma D, Leo K, Ding J, Wang L, Qiao Q, Jia H, Gnade BE. Using interlayer step-wise triplet transfer to achieve an efficient white organic light-emitting diode with high color-stability. *Appl Phys Lett* 2014;104:193303.
- [20] Ye J, Chen Z, An F, Sun M, Mo HW, Zhang X, Lee CS. Achieving highly efficient simple-emission layer fluorescence/phosphorescence hybrid white organic light-emitting devices via effective confinement of triplets. *ACS Appl Mater Interfaces* 2014;6:8964-70.
- [21] Su SJ, Gonmori E, Sasabe H, Kido J. Highly efficient organic blue-and white-light-emitting devices having a carrier- and exciton-confining structure for reduced efficiency roll-off. *Adv Mater* 2008;20:4189-94.
- [22] Lamansky S, Djurovich P, Murphy D, Abdel-Razzaq F, Lee HE, Adachi C, Burrows PE, Forrest SR, Thompson ME. Highly phosphorescent bis-cyclometalated iridium complexes: synthesis, photophysical characterization, and use in organic light emitting diodes. *J Am Chem Soc* 2001;123:4304-12.
- [23] Reineke S, Schwartz G, Walzer K, Falke M, Leo K. Highly phosphorescent organic mixed films: The effect of aggregation on triplet-triplet annihilation. *Appl Phys Lett* 2009;94:163305/1-3.
- [24] Baldo MA, Adachi C, Forrest SR. Transient analysis of organic electrophosphorescence. II. Transient analysis of triplet-triplet annihilation. *Phys Rev B* 2000;62:10967-77.
- [25] Xie HZ, Liu MW, Wang OY, Zhang XH, Lee CS, Hung LS, Lee ST, Teng PF, Kwong HL, Zheng H, Che CM. Reduction of self-quenching effect in organic electrophosphorescence emitting devices via the use of sterically hindered spacers in phosphorescence molecules. *Adv Mater* 2001;13:1245-48.
- [26] Baldo MA, Lamansky S, Burrows PE, Thompson ME, Forrest SR. Very high-efficiency green organic light-emitting devices based on electrophosphorescence. *Appl Phys Lett* 1999;75:4/1-4.

- [27] Frin KM, Iha NYM. Photoinduced isomerization and luminescence of fac-[Re(CO)<sub>3</sub>(ph<sub>2</sub>phen)(bpe)]<sup>+</sup>. *J Braz Chem Soc* 2006;17:1664-71.
- [28] Chen P, Meyer TJ. Medium effects on charge transfer in metal complexes. *Chem Rev* 1998;98:1439-77.
- [29] Karatsu T, Takahashi M, Yagai S, Kitamura A. Photophysical properties of substituted homoleptic and heteroleptic phenylimidazolinato Ir(III) complexes as a blue phosphorescent material. *Inorg Chem* 2013;52:12338-50.
- [30] Kim DH, Cho NS, Oh HY, Yang JH, Jeon WS, Park JS, Suh MC, Kwon JH. Highly efficient red phosphorescent dopants in organic light-emitting devices. *Adv Mater* 2011;23:2721-6.
- [31] Frisch MJ, Trucks GW, Schlegel HB, Scuseria GE, Robb MA, Cheeseman JR, Scalmani G, Barone V, Mennucci B, Petersson GA, Nakatsuji H, Caricato M, Li X, Hratchian HP, Izmaylov AF, Bloino J, Zheng G, Sonnenberg JL, Hada M, Ehara M, Toyota K, Fukuda R, Hasegawa J, Ishida M, Nakajima T, Honda Y, Kitao O, Nakai H, Vreven T, Montgomery JJA, Peralta JE, Ogliaro F, Bearpark M, Heyd JJ, Brothers E, Kudin KN, Staroverov VN, Kobayashi R, Normand J, Raghavachari K, Rendell A, Burant JC, Iyengar SS, Tomasi J, Cossi M, Rega N, Millam JM, Klene M, Knox JE, Cross JB, Bakken V, Adamo C, Jaramillo J, Gomperts R, Stratmann RE, Yazyev O, Austin AJ, Cammi R, Pomelli C, Ochterski JW, Martin RL, Morokuma K, Zakrzewski VG, Voth GA, Salvador P, Dannenberg JJ, Dapprich S, Daniels AD, Farkas Ö, Foresman JB, Ortiz JV, Cioslowski J, Fox DJ, Gaussian 09, Gaussian, Inc. Wallingford CT 2009.
- [32] Seo JA, Gong MS, Lee JY. High efficiency yellowish green phosphorescent emitter derived from phenylbenzothienopyridine ligand. *Org Electron* 2014;15: 2068-72.

- [33] Reineke S, Schwartz G, Walzer K, Falke M, Leo K. Highly phosphorescent organic mixed films: The effect of aggregation on triplet-triplet annihilation. *Appl Phys Lett* 2009;94:163305/1-3.
- [34] Park J, Oh H, Oh S, Kim J, Park HJ, Kim OY, Lee JY, Kang Y. Deep blue phosphorescent organic light-emitting diodes with excellent external quantum efficiency. *Org Electron* 2013;14:3228-33.
- [35] Son YH, Kim SH, Kwon JH. All-phosphorescent three-color two-stack tandem white organic light emitting diodes with high-color-rendering index values. *J Inf Disp* 2014;15:185-9.
- [36] Gong S, Chen Y, Luo J, Yang C, Zhong C, Qin J, Ma D. Bipolar tetraarylsilanes as universal hosts for blue, green, orange, and white electrophosphorescence with high efficiency and low efficiency roll-off. *Adv Funct Mater* 2011;21:1168-78.
- [37] Chou HH, Li YK, Chen YH, Chang CC, Liao CY, Cheng CH. New iridium dopants for white phosphorescent devices: enhancement of efficiency and color stability by an energy-harvesting layer. *ACS Appl Mater Interfaces* 2013;5:6168-75.
- [38] Pan B, Wang B, Wang Y, Xu P, Wang L, Chen J, Ma D. A simple carbazole-N-benzimidazole bipolar host material for highly efficient blue and single layer white phosphorescent organic light-emitting diodes. *J Mater Chem C* 2014;2:2466-9.
- [39] Wang R, Liu D, Ren H, Zhang T, Yin H, Liu G, Li J. Highly efficient orange and white organic light-emitting diodes based on new orange iridium complexes. *Adv Mater* 2011;23:2823-7.
- [40] Cui LS, Liu Y, Liu XY, Jiang ZQ, Liao LS. Design and synthesis of pyrimidine-based iridium(III) complexes with horizontal orientation for orange and white phosphorescent OLEDs. *ACS Appl Mater Interfaces* 2015;7:11007-14.

- [41] Guo LY, Zhang XL, Wang HS, Liu C, Li ZG, Liao ZJ, Mi BX, Zhou XH, Zheng C, Li YH, Gao ZQ. New homoleptic iridium complexes with C N=N type ligand for high efficiency orange and single emissive-layer white OLEDs. *J Mater Chem C* 2015;3: 5412-8.
- [42] Xie YM, Cui LS, Liu Y, Zu FS, Li Q, Jiang ZQ, Liao LS. Efficient blue/white phosphorescent organic light-emitting diodes based on a silicon-based host material via a direct carbon-nitrogen bond. *J Mater Chem C* 2015;3:5347-53.
- [43] Kim HU, Jang JH, Song W, Jung BJ, Lee JY, Hwang DH. Improved luminance and external quantum efficiency of red and white organic light-emitting diodes with iridium(III) complexes with phenyl-substituted 2-phenylpyridine as a second cyclometalated ligand. *J Mater Chem C* 2015;3:12107-15.

## Graphical Abstract

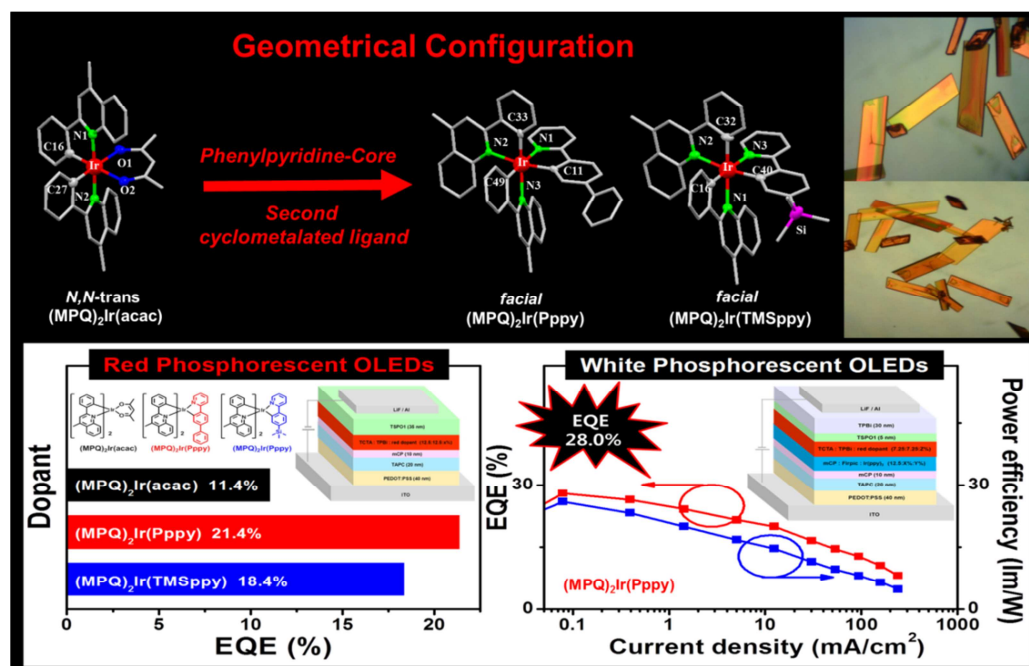


**Table captions**

Table 1. Selected bond lengths [ $\text{\AA}$ ] of  $(\text{MPQ})_2\text{Ir}(\text{acac})$ ,  $(\text{MPQ})_2\text{Ir}(\text{Pppy})$ , and  $(\text{MPQ})_2\text{Ir}(\text{TMSppy})$ .

Table 2. Summary of photophysical and electrochemical properties of synthesized iridium(III) complexes.

Table 3. Summary of performances of fabricated red phosphorescent OLEDs.

Table 4. Summary of performances of fabricated white phosphorescent OLEDs.

Table 5. Summary of device performances of WOLEDs reported in literature.

Table 1.

| (MPQ) <sub>2</sub> Ir(acac) |            | (MPQ) <sub>2</sub> Ir(Pppy) |            | (MPQ) <sub>2</sub> Ir(TMSppy) |            |
|-----------------------------|------------|-----------------------------|------------|-------------------------------|------------|
| Bond                        | Length [Å] | Bond                        | Length [Å] | Bond                          | Length [Å] |
| Ir(1)-C(16)                 | 1.978(5)   | Ir(1)-C(11)                 | 2.015(8)   | Ir(1)-C(16)                   | 2.012(4)   |
| Ir(1)-C(27)                 | 1.973(5)   | Ir(1)-C(33)                 | 1.985(8)   | Ir(1)-C(32)                   | 2.007(4)   |
| Ir(1)-N(1)                  | 2.063(4)   | Ir(1)-C(49)                 | 2.000(8)   | Ir(1)-C(40)                   | 2.009(4)   |
| Ir(1)-N(2)                  | 2.069(4)   | Ir(1)-N(1)                  | 2.142(6)   | Ir(1)-N(1)                    | 2.236(3)   |
| Ir(1)-O(1)                  | 2.166(3)   | Ir(1)-N(2)                  | 2.181(6)   | Ir(1)-N(2)                    | 2.198(3)   |
| Ir(1)-O(2)                  | 2.165(3)   | Ir(1)-N(3)                  | 2.224(7)   | Ir(1)-N(2)                    | 2.145(3)   |

Table 2.

| Dopant                             | Photophysical               |   |                                   |            | Electrochemical |           |           |
|------------------------------------|-----------------------------|---|-----------------------------------|------------|-----------------|-----------|-----------|
|                                    | $\lambda_{\text{max}}$ [nm] | $\lambda_{\text{em}}$ <sup>[a]</sup> [nm] | $\Phi_{\text{PL}}$ <sup>[b]</sup> | $E_g$ [eV] | $T_1$ [eV]      | HOMO [eV] | LUMO [eV] |
| <b>(MPQ)<sub>2</sub>Ir(acac)</b>   | 270, 338, 470               | 589/595                                   | 0.11                              | 2.09       | 2.14            | -5.21     | -3.12     |
| <b>(MPQ)<sub>2</sub>Ir(Pppy)</b>   | 271, 308, 398, 446          | 597/601                                   | 0.16                              | 2.14       | 2.13            | -5.16     | -3.02     |
| <b>(MPQ)<sub>2</sub>Ir(TMSppy)</b> | 272, 290, 402, 450          | 597/602                                   | 0.13                              | 2.12       | 2.13            | -5.13     | -3.01     |

[a] Maximum emission wavelength, measured in toluene solution ( $10^{-5}$  M) and neat film state. [b] Measured in degassed 2-methyltetrahydrofuran solution relative to (PQ)<sub>2</sub>Ir(acac) ( $\Phi_{\text{PL}} = 0.10$ ).

Table 3.

| Dopant                            | x% | $\lambda_{\max}$ , FWHM [nm] | CIE <sup>[a]</sup> (x,y) | $V_{\text{turn}}^{\text{[b]}}$ [V] | $L_{\text{max}}$ [cd/m <sup>2</sup> ] | EQE <sup>[c]</sup> [%] | CE <sup>[c]</sup> [cd/A] | PE <sup>[c]</sup> [lm/W] |
|-----------------------------------|----|------------------------------|--------------------------|------------------------------------|---------------------------------------|------------------------|--------------------------|--------------------------|
| (MPQ) <sub>2</sub> Ir<br>(acac)   | 5  | 592, 81                      | (0.59,0.41)              | 4.5                                | 5235                                  | 11.1/10.2              | 20.4/18.9                | 11.1/9.14                |
|                                   | 10 | 595, 81                      | (0.60,0.40)              | 4.5                                | 6730                                  | 6.28/6.22              | 10.9/10.8                | 5.26/4.88                |
|                                   | 15 | 597, 81                      | (0.60,0.40)              | 4.5                                | 5464                                  | 4.27/3.91              | 7.02/6.51                | 3.25/2.64                |
| (MPQ) <sub>2</sub> Ir<br>(Pppy)   | 5  | 593, 93                      | (0.57,0.43)              | 4.0                                | 9712                                  | 18.0/16.7              | 34.4/32.0                | 25.7/16.4                |
|                                   | 10 | 597, 93                      | (0.59,0.41)              | 4.0                                | 14470                                 | 18.7/16.8              | 32.5/29.4                | 19.3/14.6                |
|                                   | 15 | 600, 93                      | (0.59,0.41)              | 4.0                                | 14690                                 | 21.4/16.5              | 35.5/27.3                | 20.5/13.2                |
| (MPQ) <sub>2</sub> Ir<br>(TMSppy) | 5  | 592, 91                      | (0.57,0.42)              | 3.5                                | 7863                                  | 17.1/14.0              | 32.3/26.7                | 28.6/14.4                |
|                                   | 10 | 597, 91                      | (0.58,0.42)              | 3.5                                | 10570                                 | 17.1/13.5              | 30.7/24.5                | 26.7/12.9                |
|                                   | 15 | 600, 91                      | (0.59,0.41)              | 3.5                                | 12220                                 | 18.4/14.2              | 31.8/25.0                | 29.9/12.8                |

[a] Values measured at a luminance of 1,000 cd/m<sup>2</sup>. [b] Values measured at a luminance of 1 cd/m<sup>2</sup>. [c] Values measured at maximum efficiency and luminance of 1,000 cd/m<sup>2</sup>.

Table 4.

| Device | $V_{\text{turn}}^{\text{[a]}}$ [V] | $L_{\text{max}}$ [cd/m <sup>2</sup> ] | EQE <sup>[b]</sup> [%] | CE <sup>[b]</sup> [cd/A] | PE <sup>[b]</sup> [lm/W] | CCT <sup>[c]</sup> [K] | CIE <sup>[c]</sup> (x,y) | CRI <sup>[c]</sup> |
|--------|------------------------------------|---------------------------------------|------------------------|--------------------------|--------------------------|------------------------|--------------------------|--------------------|
| W1     | 6.0                                | 28040                                 | 22.6/17.6              | 39.9/31.0                | 19.5/12.5                | 2605                   | (0.47,0.42)              | 78                 |
| W2     | 5.5                                | 34500                                 | 26.1/22.6              | 46.7/41.1                | 23.2/17.2                | 2932                   | (0.46,0.43)              | 81                 |
| W3     | 5.5                                | 38320                                 | 28.0/23.6              | 52.3/44.8                | 26.0/19.2                | 3283                   | (0.44,0.44)              | 81                 |

<sup>a)</sup> Values measured at a luminance of 1 cd/m<sup>2</sup>. <sup>b)</sup> Values measured at maximum efficiency and luminance of 1000 cd/m<sup>2</sup>. <sup>c)</sup> Values measured at a luminance of 1000 cd/m<sup>2</sup>.

Table 5.

| Ref.      | WOLED <sup>a)</sup>       | Emissive layer<br>(dopant)   | EQE <sub>max</sub><br>(%) | CIE<br>(x,y) | CCT<br>(K) |
|-----------|---------------------------|--|---------------------------|--------------|------------|
| 36        | 2 colours (B + Y)         | Flrpic:(fbi) <sub>2</sub> Ir(acac)   | 19.1                      | (0.38,0.44)  | -          |
| 37        | 2 colours (B + Y)         | (fmoppy) <sub>2</sub> Ir(tfypyz):(dpiq) <sub>2</sub> Ir(acac)                              | 21.5                      | (0.44,0.45)  | 3239       |
| 38        | 2 colours (B + Y)         | Flrpic:(bt) <sub>2</sub> Ir(acac)  | 22.9                      | (0.39,0.45)  | 4140       |
| 39        | 2 colours (B + Y)         | Flrpic:(F-bt) <sub>2</sub> Ir(acac)  | 26.2                      | (0.35,0.44)  | -          |
| 40        | 2 colours (B + O)         | Flrpic:(dmppm) <sub>2</sub> Ir(acac)   | 28.6                      | (0.45,0.41)  | 3585       |
| 41        | 2 colours (B + O)         | Flrpic:IrNPPya   | 23.9                      | (0.33,0.46)  | -          |
| 42        | 3 colours (B + G + R)     | Flrpic:(ppy) <sub>2</sub> Ir(acac):(MDQ) <sub>2</sub> Ir(acac)                             | 21.5                      | (0.43,0.45)  | -          |
| 43        | 3 colours(B + G + R)      | Flrpic:Ir(ppy) <sub>3</sub> :(DMPQ) <sub>2</sub> Ir(Pppy)                                  | 21.9                      | (0.39,0.41)  | 4518       |
| 17        | 4 colours (B + G + O + R) | Flrpic:(ppy) <sub>2</sub> Ir(acac):(fbi) <sub>2</sub> Ir(acac):(piq) <sub>2</sub> Ir(acac) | 10.8                      | (0.45,0.45)  | 3100       |
| This work | 3 colours (B + G + R)     | Flrpic:Ir(ppy) <sub>3</sub> :(MPQ) <sub>2</sub> Ir(Pppy)                                   | 28.0                      | (0.44,0.44)  | 3283       |

[a] Component colors: B; blue, G; green, O; orange, R; red.

**Figure captions**

Fig. 1. Single-crystal and crystal-packing structures of **(MPQ)<sub>2</sub>Ir(acac)**, **(MPQ)<sub>2</sub>Ir(Pppy)**, and **(MPQ)<sub>2</sub>Ir(TMSppy)**. Solvent molecules and hydrogen atoms are omitted for clarity.

Fig. 2. (a) UV-visible absorption and (b) PL spectra of **(MPQ)<sub>2</sub>Ir(acac)**, **(MPQ)<sub>2</sub>Ir(Pppy)**, and **(MPQ)<sub>2</sub>Ir(TMSppy)**.

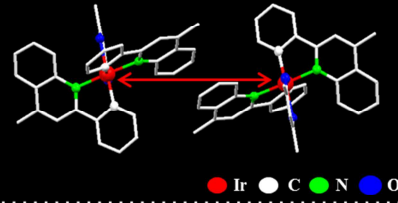
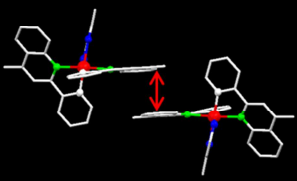
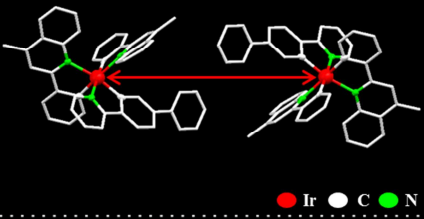
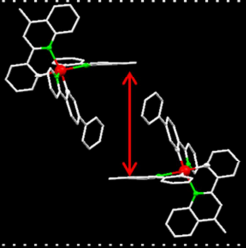
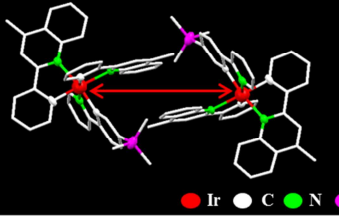
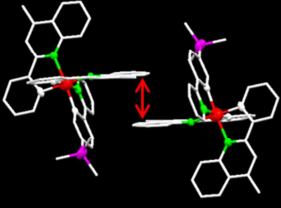
Fig. 3. Frontier molecular orbitals HOMO and LUMO of **(MPQ)<sub>2</sub>Ir(acac)**, **(MPQ)<sub>2</sub>Ir(Pppy)**, and **(MPQ)<sub>2</sub>Ir(TMSppy)** calculated using DFT on B3LYP/6-31G(d).

Fig. 4. (a) EL spectra, (b) current density-voltage-luminance (*J-V-L*), and (c) external quantum efficiency-luminance-current efficiency (EQE-*L*-CE) curves of **(MPQ)<sub>2</sub>Ir(acac)**, **(MPQ)<sub>2</sub>Ir(Pppy)**, and **(MPQ)<sub>2</sub>Ir(TMSppy)** red phosphorescent OLEDs.

Fig. 5. (a) EL spectra, (b) current density-voltage-luminance (*J-V-L*) and (c) external quantum efficiency-luminance-power efficiency (EQE-*L*-PE) curves of WOLED based on Irpic, Ir(ppy)<sub>3</sub>, and **(MPQ)<sub>2</sub>Ir(Pppy)**.

Fig. 6. CIE-X and CIE-Y values of W1, W2, and W3 devices at different driving voltages.

Fig. 1.

|                                | Crystal packing diagram  | Ir-Ir distance | Crystal packing diagram   | $\pi$ - $\pi$ distance |
|--------------------------------|--|----------------|---|------------------------|
| (MPQ) <sub>2</sub> Ir (acac)   |   | 10.80 Å        |   | 3.43 Å                 |
| (MPQ) <sub>2</sub> Ir (Pppy)   |   | 15.32 Å        |   | 9.74 Å                 |
| (MPQ) <sub>2</sub> Ir (TMSppy) |  | 10.94 Å        |  | 3.49 Å                 |

ACCEPTED

Fig. 2.

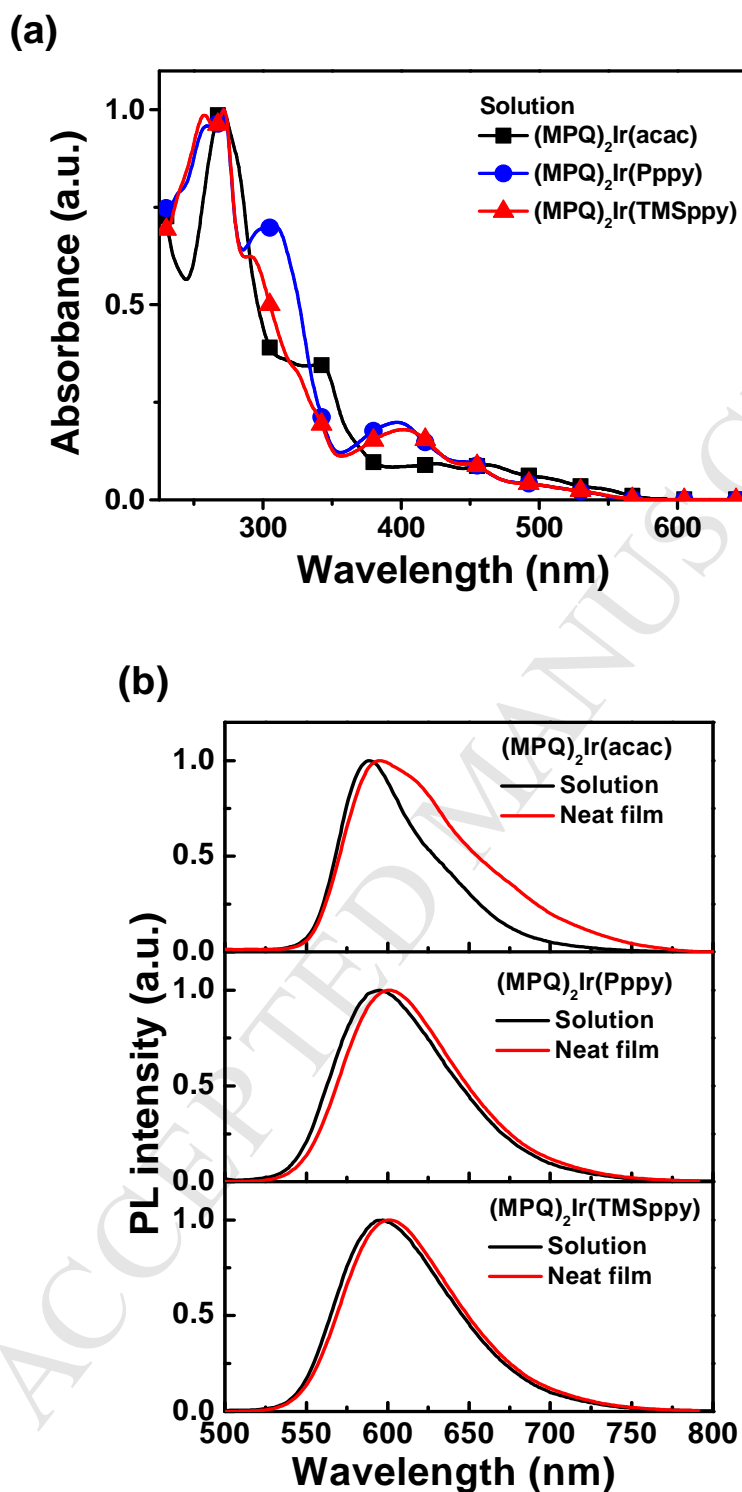


Fig. 3.

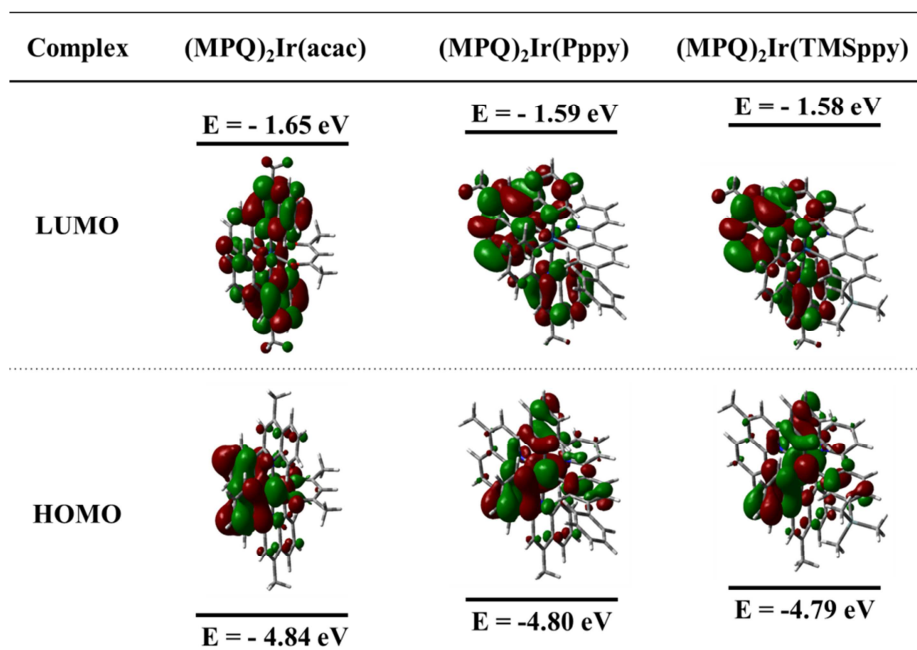


Fig.4.

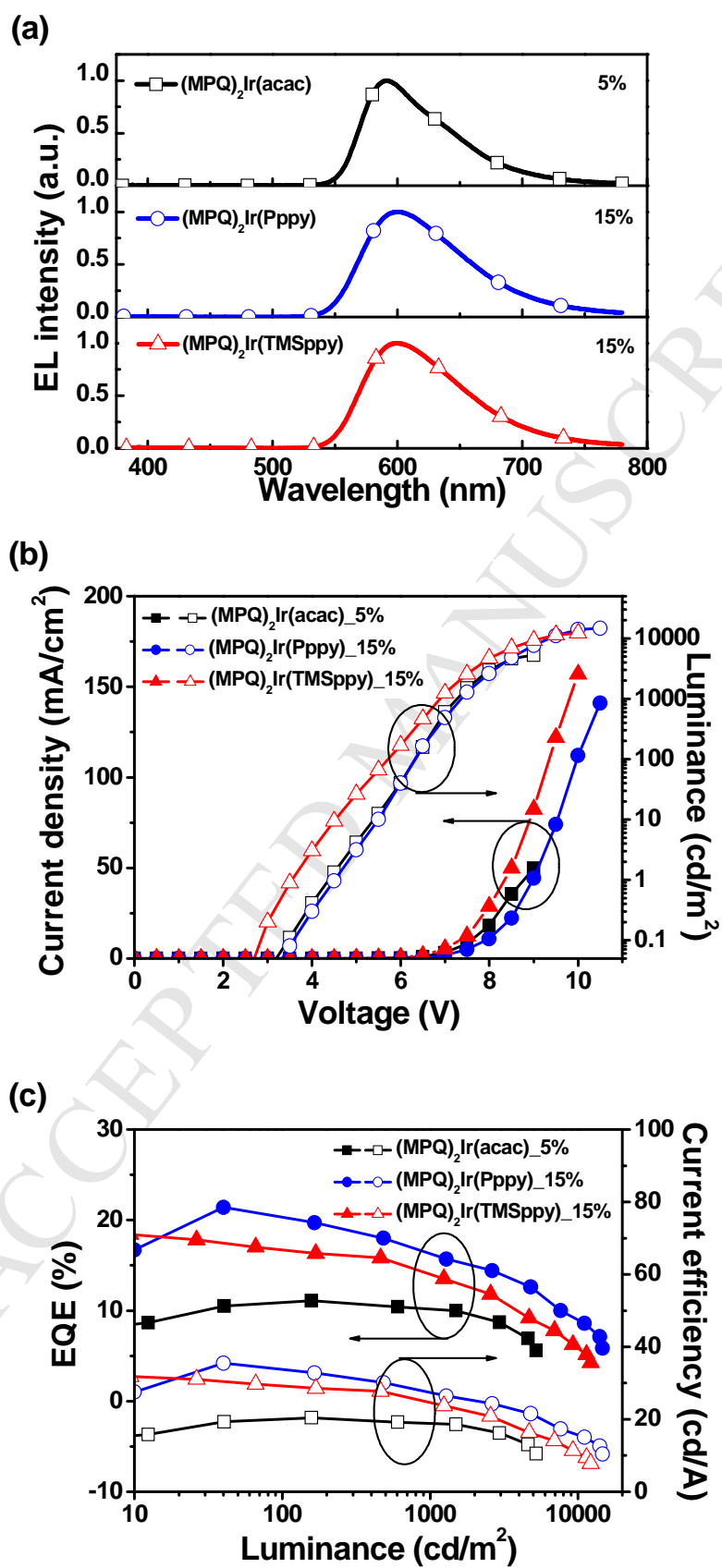


Fig. 5.

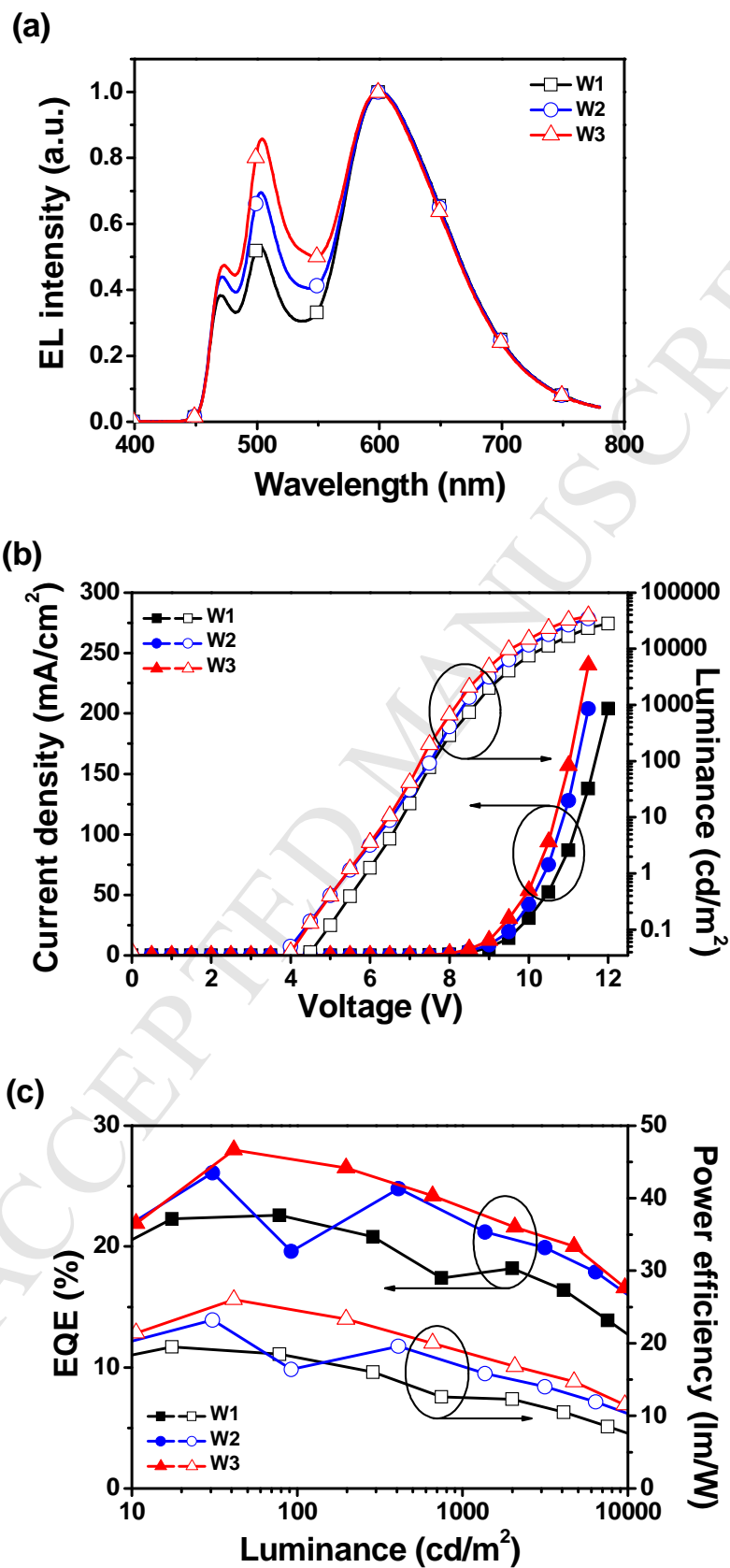
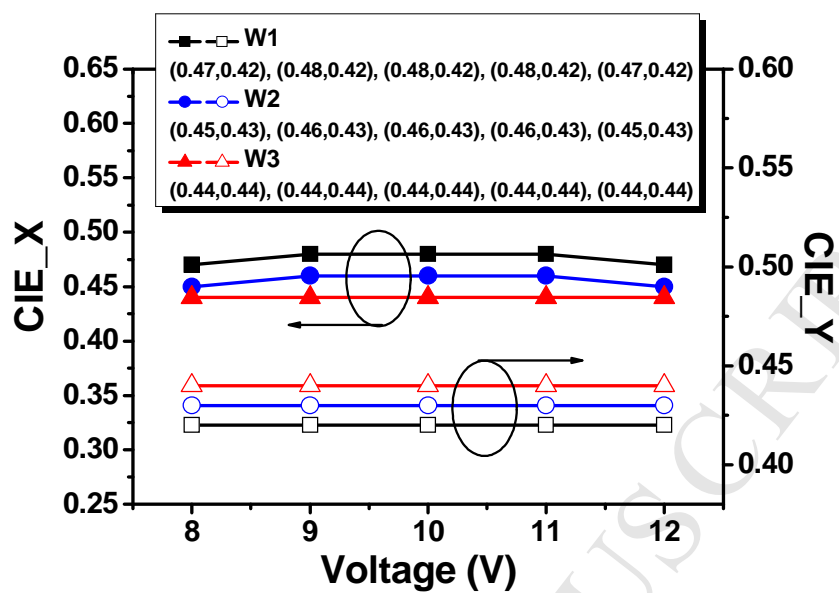


Fig. 6.



**Highlights**

- New red phosphorescent Ir(III) complexes, (MPQ)<sub>2</sub>Ir(Pppy) and (MPQ)<sub>2</sub>Ir(TMSppy) were synthesized.
- (MPQ)<sub>2</sub>Ir(Pppy) exhibited high maximum external quantum efficiency of 28.0% in WOLED.
- (MPQ)<sub>2</sub>Ir(Pppy) showed excellent spectral stability at different voltages in WOLED.